2016 IEEE International Conference on Advanced Intelligent Mechatronics (AIM)
Banff, Alberta, Canada, July 12–15, 2016

A Novel Locomotion Robot That Slides and Rotates on Slippery Downhill

Fumihiko Asano[1], Taiki Seino[1], Isao Tokuda[2] and Yuji Harata[3]

***Abstract*— This paper proposes a novel locomotion robot that slides and rotates on a slippery downhill by utilizing the dynamical effect of an actively-controlled wobbling mass. First, we introduce a 4-DOF seedlike robot model that consists of two identical arc-shaped body frames and a short link, and develop the equation of motion, friction dynamics, and control law for generating a wobbling motion. Second, we numerically show that a stable downward motion can be generated based on the effect of entrainment to the wobbling motion at high frequencies on a slippery downhill. Third, we analyze the fundamental properties of the generated motion, such as moving speed and ground reaction force, through numerical simulations. Throughout this paper, we show that the robot's arc-shaped body frame can maintain kinetic energy or rotation motion without stopping on the high-frictional downhill, and that this property also enables the indirect control of the moving speed by utilizing the wobbling effect.**

I. INTRODUCTION

Achieving high adaptation ability to various road surface conditions is the most essential function for practicable locomotion robots. Adaptation to slippery road surface is one of the most difficult issues in robot locomotion control [1][2]. It is obviously difficult to walk stably on a frozen road surface, and we usually walk in spiked shoes. This increases, however, the probability of damage to the road surface. It is therefore more difficult to walk on without slipping and without scratching the surface.

Based on the considerations, this paper proposes a novel locomotion robot for achieving stable forward (downward) motion without scratching the frozen road surface of a downhill based on indirectly control of a wobbling mass actively driven in the robot body [3][4]. As the first step, in this paper we consider a simple robot model that consists of two identical arc-shaped body frames and a wobbling mass as a single link. First, we develop the mathematical model of the robot, and consider an output following control for achieving the desired active wobbling motion. The sliding friction model is specified as the Coulomb friction [1][2]. Second, we introduce a simple time-dependent (sinusoidal) trajectory for generating an active wobbling motion, and numerically show that the robot's downward motion is entrained to it at high frequencies. Third, we perform parametric studies through numerical simulations and discuss how the gait properties change according to the physical and control parameters.

The most significant feature of the novel locomotion robot the authors propose is to maintain the generated rotational kinetic energy on the high-frictional downhill while slightly sliding. In the case of a point-mass moving along the high-frictional downhill, the sliding motion stops in seconds. In the case of the arc-shaped body frame, however, the sliding speed changes very little and the translational motion can be indirectly controlled by utilizing the active wobbling effect. These properties are of scientific interest and hold enormous potentialities as a novel locomotion system.

[1]Fumihiko Asano and Taiki Seino are with the School of Information Science, Japan Advanced Institute of Science and Technology, 1-1 Asahidai, Nomi, Ishikawa 923-1292, Japan {fasano,s1510028}@jaist.ac.jp

[2]Isao Tokuda is with the Department of Mechanical Engineering, Faculty of Science and Engineering, Ritsumeikan University, 1-1-1 Nojihigashi, Kusatsu, Shiga 525-8577, Japan isao@fc.ritsumei.ac.jp

[3]Yuji Harata is with the Division of Mechanical Systems and Applied Mechanics, Faculty of Engineering, Hiroshima University, 1-4-1, Kagamiyama, Higashi-Hiroshima, Hiroshima 739-8527, Japan harata@hiroshima-u.ac.jp

II. DYNAMICS AND CONTROL

A. Equation of Motion

Fig. 1 illustrates the 4-DOF robot model this paper considers. This seedlike robot consists of two identical arc-shaped body frames whose radius is R [m] and a single-link wobbling mass actively controlled in the body. Here, (x, z) is the central position of the lower body surface, θ_1 and θ_2 are the angular positions of the body and wobbling mass with respect to vertical. ϕ [rad] is the slope angle. We assume that the robot always contacts the slope surface on one point and always slides on it. The center of mass (CoM) of the whole body is positioned at its central point, and the mass is m_1 [kg] and the inertial moment about it is I [kg·m^2]. The wobbling mass is m_2 [kg] and its inertia moment is zero. a

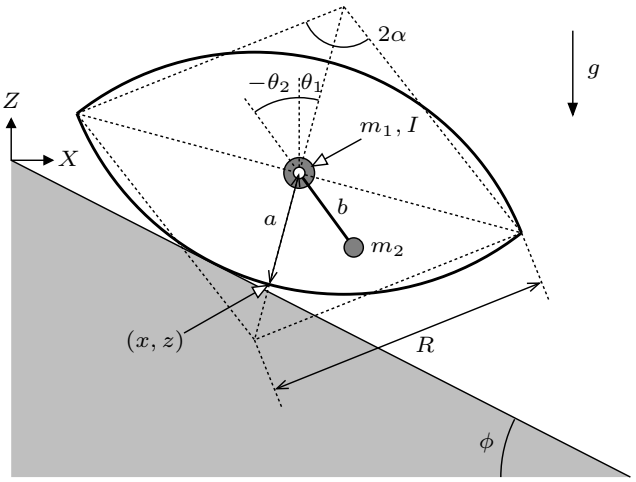

Fig. 1. Robot model

[m] is the length between the central position of the whole body and the (x, z). b [m] is the length of the wobbling mass and is chosen as shorter than a. 2α [rad] is the central angle for the sector, and this is uniquely determined by the values of a and R.

As described in the subsequent sections, this robot can move down the slope utilizing the internal machinery vibration. The robot shape should be optimally-designed so that it can utilize the body surface skillfully during motion like dynamic manipulation systems [5]. In this paper, however, we consider the arc-shaped body for development of the simplest mathematical model.

Let $\boldsymbol{q} = \begin{bmatrix} x & z & \theta_1 & \theta_2 \end{bmatrix}^{\mathrm{T}}$ be the generalized coordinate vector. The robot equation of motion then becomes

$$\boldsymbol{M}(\boldsymbol{q})\ddot{\boldsymbol{q}} + \boldsymbol{h}(\boldsymbol{q}, \dot{\boldsymbol{q}}) = \boldsymbol{S}u + \boldsymbol{J}(\boldsymbol{q})^{\mathrm{T}}\lambda + \boldsymbol{J}_{\mu}(\boldsymbol{q}, \dot{\boldsymbol{q}})^{\mathrm{T}}\lambda. \quad (1)$$

The details of the left-hand-side terms are as follows.

$$\boldsymbol{M}(\boldsymbol{q}) = \begin{bmatrix} M & 0 & Ma\cos\theta_1 & M_{14} \\ 0 & M & -Ma\sin\theta_1 & M_{24} \\ Ma\cos\theta_1 & -Ma\sin\theta_1 & Ma^2 + I & M_{34} \\ M_{14} & M_{24} & M_{34} & m_2b^2 \end{bmatrix}$$

$$M = m_1 + m_2,\ M_{14} = -m_2b\cos\theta_2$$

$$M_{24} = m_2b\sin\theta_2,\ M_{34} = -m_2ab\cos(\theta_1 - \theta_2)$$

$$\boldsymbol{h}(\boldsymbol{q}, \dot{\boldsymbol{q}}) = \begin{bmatrix} m_2b\dot{\theta}_2^2\sin\theta_2 - Ma\dot{\theta}_1^2\sin\theta_1 \\ m_2b\dot{\theta}_2^2\cos\theta_2 - Ma\dot{\theta}_1^2\cos\theta_1 + Mg \\ -m_2ab\dot{\theta}_2^2\sin(\theta_1 - \theta_2) - Mag\sin\theta_1 \\ m_2ab\dot{\theta}_1^2\sin(\theta_1 - \theta_2) + m_2bg\sin\theta_2 \end{bmatrix}$$

We assume that the robot can exert a joint torque between the body frame and wobbling mass. Therefore the driving vector should be $\boldsymbol{S} = \begin{bmatrix} 0 & 0 & 1 & -1 \end{bmatrix}^{\mathrm{T}}$.

The contact position is specified as

$$\begin{bmatrix} \bar{x} \\ \bar{z} \end{bmatrix} = \begin{bmatrix} x + R\sin\theta_1 - R\sin\phi \\ z + R\cos\theta_1 - R\cos\phi \end{bmatrix}, \quad (2)$$

and its time derivative becomes

$$\frac{\mathrm{d}}{\mathrm{d}t}\begin{bmatrix} \bar{x} \\ \bar{z} \end{bmatrix} = \begin{bmatrix} \dot{x} + R\dot{\theta}_1\cos\theta_1 \\ \dot{z} - R\dot{\theta}_1\sin\theta_1 \end{bmatrix}. \quad (3)$$

The velocity constraint condition for the contact position is given by

$$\dot{\bar{z}} = -\dot{\bar{x}}\tan\phi. \quad (4)$$

Following Eqs. (3) and (4), we get

$$\dot{x}\tan\phi + \dot{z} + R\dot{\theta}_1\left(\cos\theta_1\tan\phi - \sin\theta_1\right) = 0, \quad (5)$$

and this can be arranged to

$$\begin{bmatrix} \tan\phi & 1 & R\left(\cos\theta_1\tan\phi - \sin\theta_1\right) & 0 \end{bmatrix}\dot{\boldsymbol{q}} = 0. \quad (6)$$

In the following, we denote Eq. (6) as

$$\boldsymbol{J}(\boldsymbol{q})\dot{\boldsymbol{q}} = 0, \quad (7)$$

and this is the holonomic constraint condition.

B. Sliding Friction Model

From the detail of $\boldsymbol{J}(\boldsymbol{q})$ in Eq. (6), we can understand that the vertical ground reaction force is λ and the horizontal one is $\lambda\tan\phi$, and that the magnitude of the net (total) ground reaction force becomes $\lambda/\cos\phi$ and this is normal to the slope as illustrated in Fig. 2. The sliding frictional force vector, $\boldsymbol{J}_{\mu}(\boldsymbol{q}, \dot{\boldsymbol{q}})^{\mathrm{T}}\lambda \in \mathbb{R}^4$ in Eq. (1), represented as the Coulomb friction model is determined as follows. As seen in Fig. 2, the 2D frictional force vector is given by

$$\begin{bmatrix} \cos\phi \\ -\sin\phi \end{bmatrix}\frac{\mu\lambda}{\cos\phi},$$

where μ is the signed frictional coefficient described later. Note that μ becomes negative in the case that the contact position's velocity tangential to the slope is positive and vice versa. Fig. 2 illustrates the case that the μ is negative. The rotational moment generated by the frictional force can be calculated as the following outer product.

$$\begin{aligned} &\begin{bmatrix} \bar{x} - x \\ 0 \\ \bar{z} - z \end{bmatrix} \times \begin{bmatrix} \cos\phi \\ 0 \\ -\sin\phi \end{bmatrix}\frac{\mu\lambda}{\cos\phi} \\ &= \begin{bmatrix} R\left(\sin\theta_1 - \sin\phi\right) \\ 0 \\ R\left(\cos\theta_1 - \cos\phi\right) \end{bmatrix} \times \begin{bmatrix} \mu \\ 0 \\ -\mu\tan\phi \end{bmatrix}\lambda \\ &= \begin{bmatrix} 0 \\ \mu R\left(\cos(\phi - \theta_1) - 1\right)/\cos\phi \\ 0 \end{bmatrix}\lambda \end{aligned} \quad (8)$$

The frictional force vector then becomes

$$\boldsymbol{J}_{\mu}(\boldsymbol{q}, \dot{\boldsymbol{q}})^{\mathrm{T}}\lambda = \begin{bmatrix} \mu \\ -\mu\tan\phi \\ \mu R\left(\cos(\phi - \theta_1) - 1\right)/\cos\phi \\ 0 \end{bmatrix}\lambda. \quad (9)$$

The only difference in $\boldsymbol{J}_{\mu}(\boldsymbol{q}, \dot{\boldsymbol{q}})$ between the point-footed compass-like biped robot [2] and semicircular-footed one or seedlike robot is the third component; the rotational moment for the θ_1. This dynamical effect creates an interesting motion as described later.

The signed frictional coefficient, μ, is a function of the sliding velocity defined as follows.

$$\begin{aligned} \mu &= -\mu_0\mathrm{sign}\left(\frac{\dot{\bar{x}}}{\cos\phi} - R\dot{\theta}_1\right) \\ &= -\mu_0\mathrm{sign}\left(\frac{\dot{x} + R\dot{\theta}_1\cos\theta_1}{\cos\phi} - R\dot{\theta}_1\right) \\ &= -\mu_0\mathrm{sign}\left(\dot{x} + R\dot{\theta}_1\left(\cos\theta_1 - \cos\phi\right)\right) \end{aligned} \quad (10)$$

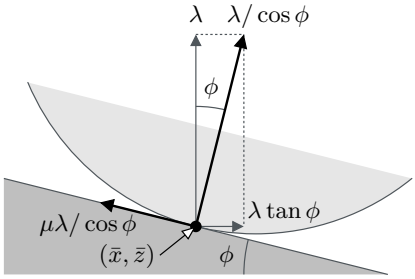

Fig. 2. Ground reaction and sliding friction forces

Here, $\dot{\tilde{x}}/\cos\phi$ [m/s] is the contact position's velocity tangential to the slope, and μ_0 is a positive constant that gives the maximum magnitude of the μ. We should give careful attention to find the sliding velocity. Without going into detail, the rotational velocity at contact point, $R\dot{\theta}_1$, must be subtracted from actual velocity at the point, $\dot{\tilde{x}}/\cos\phi$. A similar problem was discussed in [6].

To avoid chattering about

$$\begin{aligned}&\mu = -\mu_0 \mathrm{sign}\left(\dot{x} + R\dot{\theta}_1(\cos\theta_1 - \cos\phi)\right) = 0\\ &\iff \dot{x} = -R\dot{\theta}_1(\cos\theta_1 - \cos\phi),\end{aligned} \tag{11}$$

in this paper we consider the following smooth function.

$$\mu = -\mu_0 \tanh\left(c\left(\frac{\dot{x} + R\dot{\theta}_1\cos\theta_1}{\cos\phi} - R\dot{\theta}_1\right)\right) \tag{12}$$

Here, c is a positive constant that adjusts the sharpness of $\tanh$.

From Eq. (8), we can understand that the frictional force generates the clockwise rotational moment for θ_1 if $\dot{x} > -R\dot{\theta}_1(\cos\theta_1 - \cos\phi)$ and ϕ is sufficiently small, and vice versa.

C. Ground Reaction Force

By solving the simultaneous equations (1) and time-derivative of (7) for the Lagrange's undetermined multiplyer λ, we get

$$\begin{aligned}\lambda =\ & -X(\boldsymbol{q},\dot{\boldsymbol{q}})^{-1}\left(\boldsymbol{J}(\boldsymbol{q})\boldsymbol{M}(\boldsymbol{q})^{-1}\left(\boldsymbol{S}u - \boldsymbol{h}(\boldsymbol{q},\dot{\boldsymbol{q}})\right)\right)\\ & -X(\boldsymbol{q},\dot{\boldsymbol{q}})^{-1}\dot{\boldsymbol{J}}(\boldsymbol{q},\dot{\boldsymbol{q}})\dot{\boldsymbol{q}},\end{aligned} \tag{13}$$

where

$$\hat{\boldsymbol{J}}(\boldsymbol{q},\dot{\boldsymbol{q}}) := \boldsymbol{J}(\boldsymbol{q}) + \boldsymbol{J}_\mu(\boldsymbol{q},\dot{\boldsymbol{q}}), \tag{14}$$

$$X(\boldsymbol{q},\dot{\boldsymbol{q}}) := \boldsymbol{J}(\boldsymbol{q})\boldsymbol{M}(\boldsymbol{q})^{-1}\hat{\boldsymbol{J}}(\boldsymbol{q},\dot{\boldsymbol{q}})^{\mathrm{T}}. \tag{15}$$

By substituting Eq. (13) into Eq. (1), we can arrange it to

$$\begin{aligned}\boldsymbol{M}(\boldsymbol{q})\ddot{\boldsymbol{q}} =\ & \boldsymbol{Y}(\boldsymbol{q},\dot{\boldsymbol{q}})\left(\boldsymbol{S}u - \boldsymbol{h}(\boldsymbol{q},\dot{\boldsymbol{q}})\right)\\ & -\hat{\boldsymbol{J}}(\boldsymbol{q},\dot{\boldsymbol{q}})^{\mathrm{T}}X(\boldsymbol{q},\dot{\boldsymbol{q}})^{-1}\dot{\boldsymbol{J}}(\boldsymbol{q},\dot{\boldsymbol{q}})\dot{\boldsymbol{q}},\end{aligned} \tag{16}$$

where

$$\boldsymbol{Y}(\boldsymbol{q},\dot{\boldsymbol{q}}) := \boldsymbol{I}_4 - \hat{\boldsymbol{J}}(\boldsymbol{q},\dot{\boldsymbol{q}})^{\mathrm{T}}X(\boldsymbol{q},\dot{\boldsymbol{q}})^{-1}\boldsymbol{J}(\boldsymbol{q})\boldsymbol{M}(\boldsymbol{q})^{-1}. \tag{17}$$

In this paper, we assume that $\lambda > 0$ is one of the necessary conditions in generating a stable sliding gait.

D. Output Following Control for Generating Wobbling Motion

Let $y := \boldsymbol{S}^{\mathrm{T}}\boldsymbol{q} = \theta_1 - \theta_2$ be the control output. The second-order derivative with respect to time then becomes

$$\begin{aligned}\ddot{y} =\ & \boldsymbol{S}^{\mathrm{T}}\ddot{\boldsymbol{q}}\\ =\ & \boldsymbol{S}^{\mathrm{T}}\boldsymbol{M}(\boldsymbol{q})^{-1}\boldsymbol{Y}(\boldsymbol{q},\dot{\boldsymbol{q}})\left(\boldsymbol{S}u - \boldsymbol{h}(\boldsymbol{q},\dot{\boldsymbol{q}})\right)\\ & -\boldsymbol{S}^{\mathrm{T}}\boldsymbol{M}(\boldsymbol{q})^{-1}\hat{\boldsymbol{J}}(\boldsymbol{q},\dot{\boldsymbol{q}})^{\mathrm{T}}X(\boldsymbol{q},\dot{\boldsymbol{q}})^{-1}\dot{\boldsymbol{J}}(\boldsymbol{q},\dot{\boldsymbol{q}})\dot{\boldsymbol{q}}\\ =\ & A(\boldsymbol{q},\dot{\boldsymbol{q}})u + B(\boldsymbol{q},\dot{\boldsymbol{q}}),\end{aligned}$$

where

$$\begin{aligned}A(\boldsymbol{q},\dot{\boldsymbol{q}}) :=\ & \boldsymbol{S}^{\mathrm{T}}\boldsymbol{M}(\boldsymbol{q})^{-1}\boldsymbol{Y}(\boldsymbol{q},\dot{\boldsymbol{q}})\boldsymbol{S},\\ B(\boldsymbol{q},\dot{\boldsymbol{q}}) :=\ & -\boldsymbol{S}^{\mathrm{T}}\boldsymbol{M}(\boldsymbol{q})^{-1}\boldsymbol{Y}(\boldsymbol{q},\dot{\boldsymbol{q}})\boldsymbol{h}(\boldsymbol{q},\dot{\boldsymbol{q}})\\ & -\boldsymbol{S}^{\mathrm{T}}\boldsymbol{M}(\boldsymbol{q})^{-1}\hat{\boldsymbol{J}}(\boldsymbol{q},\dot{\boldsymbol{q}})^{\mathrm{T}}X(\boldsymbol{q},\dot{\boldsymbol{q}})^{-1}\dot{\boldsymbol{J}}(\boldsymbol{q},\dot{\boldsymbol{q}})\dot{\boldsymbol{q}}.\end{aligned}$$

In this paper, we intuitively consider the following time-dependent desired trajectory for y.

$$y_{\mathrm{d}}(t) = A_m\sin(\omega t) \tag{18}$$

Here, A_m [rad] is the desired amplitude of the sinusoidal wave and ω [rad/s] is the desired angular frequency.

Then we can determine the control input for achieving $y \to y_{\mathrm{d}}(t)$ as follows.

$$u = A(\boldsymbol{q},\dot{\boldsymbol{q}})^{-1}\left(v - B(\boldsymbol{q},\dot{\boldsymbol{q}})\right) \tag{19}$$

$$v = \ddot{y}_{\mathrm{d}}(t) + K_D\left(\dot{y}_{\mathrm{d}}(t) - \dot{y}\right) + K_P\left(y_{\mathrm{d}}(t) - y\right) \tag{20}$$

Here, K_P and K_D are PD gains and are positive constants.

E. Mechanical Energy and Friction Term

The robot's total mechanical energy is given by

$$E = \frac{1}{2}\dot{\boldsymbol{q}}^{\mathrm{T}}\boldsymbol{M}(\boldsymbol{q})\dot{\boldsymbol{q}} + P(\boldsymbol{q}), \tag{21}$$

where $P(\boldsymbol{q}) = Mg(z + a\sin\theta_1) - m_2gb\sin\theta_2$ is the potential energy. The time-derivative of E becomes

$$\begin{aligned}\dot{E} =\ & \dot{\boldsymbol{q}}^{\mathrm{T}}\left(\boldsymbol{S}u + \boldsymbol{J}(\boldsymbol{q})^{\mathrm{T}}\lambda + \boldsymbol{J}_\mu(\boldsymbol{q},\dot{\boldsymbol{q}})^{\mathrm{T}}\lambda\right)\\ =\ & \dot{\boldsymbol{q}}^{\mathrm{T}}\boldsymbol{S}u + \dot{\boldsymbol{q}}^{\mathrm{T}}\boldsymbol{J}_\mu(\boldsymbol{q},\dot{\boldsymbol{q}})^{\mathrm{T}}\lambda\\ =\ & \dot{y}u + \boldsymbol{J}_\mu(\boldsymbol{q},\dot{\boldsymbol{q}})\dot{\boldsymbol{q}}\lambda.\end{aligned} \tag{22}$$

Here, however, we used the condition of Eq. (7). The first term in Eq. (22) is the input power and the second one is the time rate of change in mechanical energy according to the friction force.

In the case that the frictional coefficient of Eq. (10) is used, the second term in Eq. (22) becomes

$$\begin{aligned}\boldsymbol{J}_\mu(\boldsymbol{q},\dot{\boldsymbol{q}})\dot{\boldsymbol{q}}\lambda =\ & \mu\lambda\left(\dot{x} - \dot{z}\tan\phi\right)\\ & + \frac{\mu\lambda R\dot{\theta}_1\left(\cos(\phi - \theta_1) - 1\right)}{\cos\phi}\\ =\ & \frac{\mu\lambda\left(\dot{x} + R\dot{\theta}_1(\cos\theta_1 - \cos\phi)\right)}{\cos^2\phi}\\ =\ & -\frac{\mu_0\lambda}{\cos^2\phi}\left(\dot{x} + R\dot{\theta}_1(\cos\theta_1 - \cos\phi)\right)\\ & \times\mathrm{sign}\left(\dot{x} + R\dot{\theta}_1(\cos\theta_1 - \cos\phi)\right)\\ =\ & -\frac{\mu_0\lambda}{\cos^2\phi}\left|\dot{x} + R\dot{\theta}_1(\cos\theta_1 - \cos\phi)\right| \le 0.\end{aligned}$$

Therefore we can understand that the sliding friction always dissipates mechanical energy. Note that we used Eq. (5) for eliminating $\dot{z}$. The frictional coefficient model of Eq. (12) satisfies the same inequality.

III. GAIT GENERATION

The robot starts sliding locomotion from the following initial conditions.

$$\boldsymbol{q}(0) = \begin{bmatrix} 0 & 0 & \phi & \phi \end{bmatrix}^{\mathrm{T}}, \quad \dot{\boldsymbol{q}}(0) = \begin{bmatrix} 0 & 0 & 0 & 0 \end{bmatrix}^{\mathrm{T}} \tag{23}$$

Therefore the robot does not have the initial kinetic energy but has a small rotational moment. The system parameters are chosen as listed in Table I.

Fig. 3 shows the stick diagram for the first motion generated where $\mu_0 = 0.10$, $A_m = 0.00$ [rad], and $\omega = 0$ [rad/s]. Here, the body frame is plotted in red, its central point (active joint position) is plotted in blue, and the wobbling mass is plotted in green, respectively. Since $\tan\phi > \mu_0$ holds, the sliding motion of a point mass diverges. From Fig. 3, we can see that the robot slides down the slippery road surface while rotating and that the sliding speed monotonically increases as is the case in a point mass.

Fig. 4 shows (a) the stick diagram and (b) the trajectory of (x, z) in the generated motion for $0 \leq t \leq 10$ [s] where $\mu_0 = 0.30$, $A_m = 0.00$ [rad], and $\omega = 0$ [rad/s]. From the figures, we can see that the robot oscillates without moving the contact position. Without going into detail, however, the contact position slightly moves down and the total mechanical energy accordingly decreases. In the cases of a point-mass, the sliding speed and kinetic energy converge to zero in seconds on the high-frictional downhill ($\tan\phi < \mu_0$). In this robot, however, the generated kinetic energy is maintained for long periods without stopping the sliding motion. This intriguing property comes from the curved shape of the robot body frame.

Fig. 5 shows (a) the stick diagram and (b) the trajectory of (x, z) in the generated motion for $0 \leq t \leq 10$ [s] where $\mu_0 = 0.30$, $A_m = 0.30$ [rad], and $\omega = 50$ [rad/s]. We can see that the robot moves downward while sliding and rotating. The rotation motion can be also confirmed from Fig. 5 (b); the body frame oscillates four times in ten seconds. Although the details are omitted, the motion converges to a limit cycle and the steady motion is similar to the first one shown in Fig. 5.

TABLE I
PARAMETER SETTINGS

m_1	1.0	kg
m_2	0.2	kg
I	0.1	kg·m^2
a	0.20	m
b	0.03	m
R	0.30	m

ϕ	0.2	rad
c	10000	-
K_P	2500	s^{-2}
K_D	10000	s^{-1}

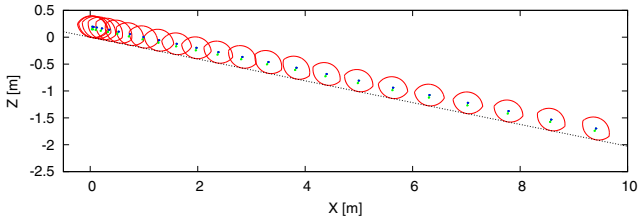

Fig. 3. Stick diagram for first motion where $A_m = 0.00$ [rad] and $\mu_0 = 0.10$

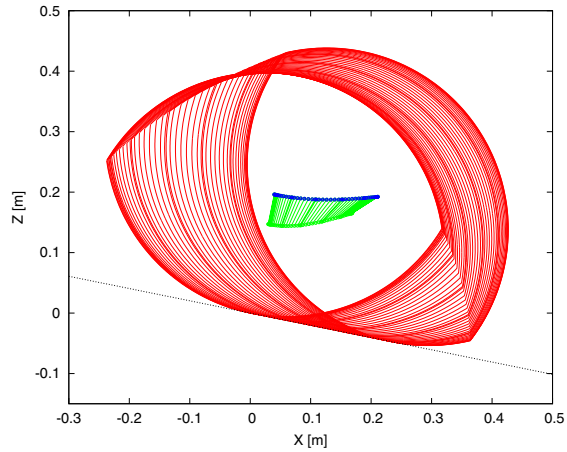

(a) Stick diagram

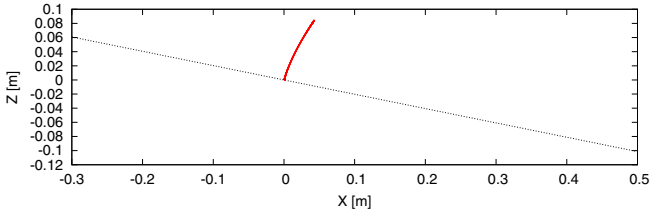

(b) Trajectory of (x, z)

Fig. 4. Stick diagram and trajectory of (x, z) for $0 \leq t \leq 10$ [s] where $A_m = 0.00$ [rad] and $\mu_0 = 0.30$

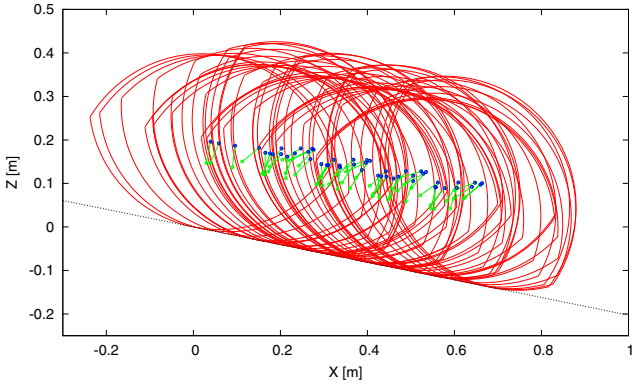

(a) Stick diagram

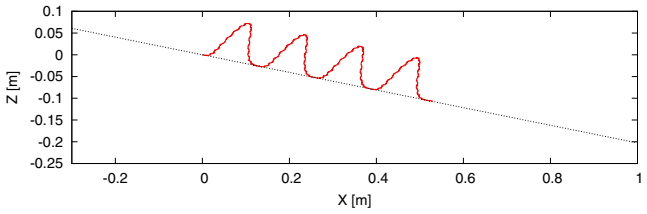

(b) Trajectory of (x, z)

Fig. 5. Stick diagram and trajectory of (x, z) for $0 \leq t \leq 10$ [s] where $A_m = 0.30$ [rad] and $\mu_0 = 0.30$

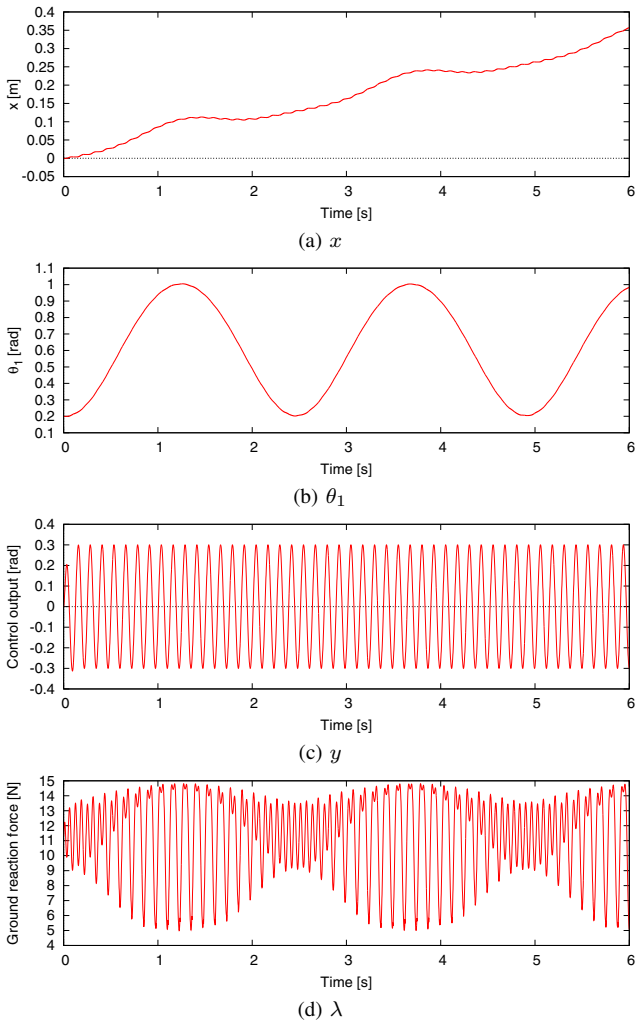

(a) x (b) θ_1 (c) y (d) λ

Fig. 6. Simulation results of sliding locomotion

Fig. 6 shows the simulation results for $0 \leq t \leq 6$ [s] where $\mu_0 = 0.30$, $A_m = 0.30$ [rad], and $\omega = 50$ [rad/s]. Here, (a) is the X-position of the contact point x, (b) the angular position of the body frame θ_1, (c) the control output y, and (d) the ground reaction force λ. Fig. 6 (b) shows that the body angle exhibits low-frequency oscillation although it is hard to be understood visually from the stick diagram. The generated trajectory of x in Fig. 6 (a) shows that a vibration of high frequency caused by the active wobbling appears in it. Fig. 6 (d) shows that the ground reaction force exhibits high-frequency oscillation according to the active wobbling motion, but is always kept positive and unilateral constraint condition is met.

IV. PARAMETRIC STUDY

A. Gait Descriptors

Preparatory for gait analysis, we define some evaluation indices.

The moving speed parallel to the slope is defined as

$$V := \frac{1}{T_e - T_s} \int_{T_s}^{T_e} \frac{\dot{x}}{\cos\phi} \mathrm{d}t, \tag{24}$$

where T_s and T_e [s] are the starting and ending times for calculation. In this paper, we choose T_s as 200, 210, $\cdots$, 290 [s] and T_e as 205, 215, $\cdots$, 295 [s].

As mentioned in the introduction, one of the purposes of this study is to develop a robot system that can skillfully locomote on a slippery floor without scratching the surface. Therefore it is important to generate the motion taking the magnitude of the ground reaction force into account in realities. The average ground reaction force is defined as

$$\Lambda := \frac{1}{T_e - T_s} \int_{T_s}^{T_e} \lambda \, \mathrm{d}t, \tag{25}$$

where λ is given by Eq. (13).

B. Computational Procedure

We perform numerical simulations based on the following computational procedure.

(P1) Set the slope angle ϕ to 0.20 [rad] and the system parameters except b to those in Table I.
(P2) Run the numerical simulation from the initial conditions of Eq. (23) for four values of b.
(P3) After elapsing 200 [s], save the gait descriptors for 10 steps.
(P4) By setting ω to $\omega+1$, repeat from (P2) as long as stable motion can be generated.

As previously mentioned, however, we assume that the ground reaction force given by Eq. (13) is kept positive during simulations.

C. Analysis Results

Fig. 7 shows the average moving speeds, V, for 10 steps after elapsing 200 seconds versus ω for four values of b, whereas Fig. 8 shows the mean values with error bars. Here, the dense plots of V represent a sign of quasi-periodic motion. The mean value of V, however, remains in a similar range in all cases. In the quasi-periodic motion, the rotation motion at nearly-fixed position is the dominant dynamics. As ω increases, V changes to monotonically increase at an almost constant rate and shows a periodic-like motion. In addition, we can see that the effects of entrainment and speeding-up are higher in long b. In the periodic motion, the dominant dynamics is the vibratory motion of the wobbling mass at a high-frequency. In addition, we can see that V is positive where $\omega = 0$ [rad/s] or the robot slightly moves downward without using the wobbling effect. In this motion, the dynamical effects of both sliding and rotating are balanced and are not acting in a dominant fashion.

Fig. 9 shows the average ground reaction forces, Λ, for 10 steps after elapsing 200 seconds versus ω for four values of b corresponding to Fig. 7, whereas Fig. 10 shows the mean values with error bars. We can see from Fig. 9 that the values are scattered in all cases. The mean values are, however, about the same in all cases. Without going into detail, the Λ is mainly determined not by b but by m_2, and we can conclude that Λ changes little for full range of ω.

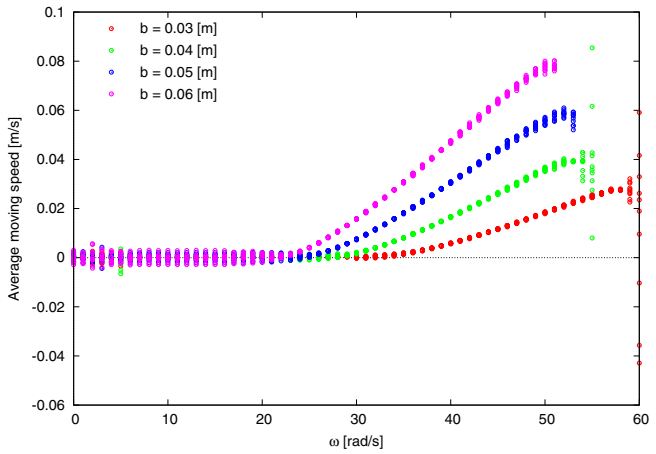

Fig. 7. Average moving speeds for 10 steps after elapsing 200 seconds versus ω for four values of b

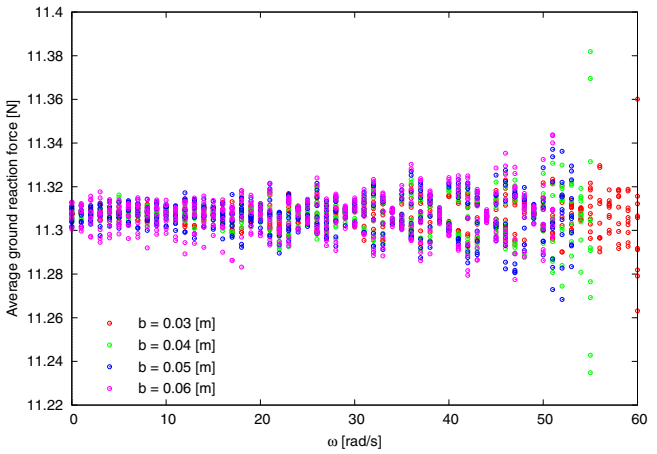

Fig. 9. Average ground reaction forces for 10 steps after elapsing 200 seconds versus ω for four values of b

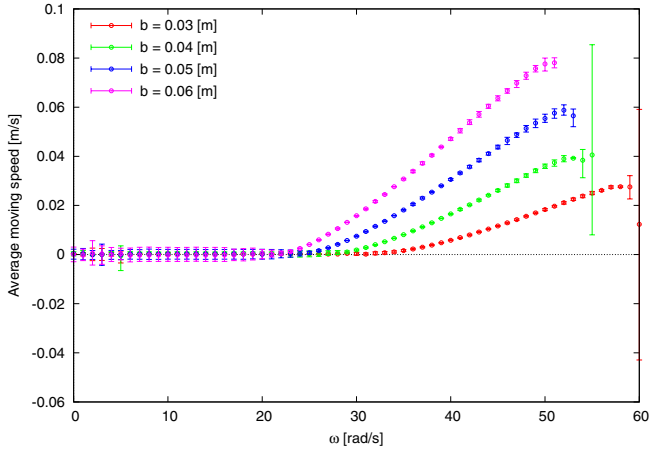

Fig. 8. Mean values of average moving speeds for 10 steps after elapsing 200 seconds versus ω for four values of b

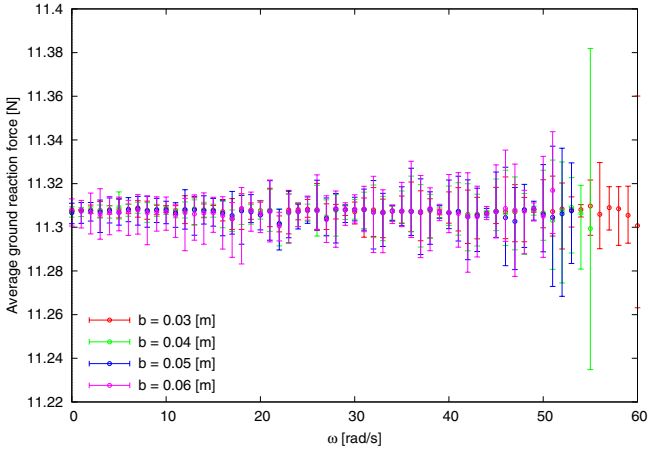

Fig. 10. Mean values of average ground reaction forces for 10 steps after elapsing 200 seconds versus ω for four values of b

V. CONCLUSION AND FUTURE WORK

In this paper, we proposed a novel locomotion robot that slides and rotates on a slippery downhill by utilizing oscillation effect of an active wobbling mass driven in the body. It was numerically shown that the generated robot motion changes from the pseudo-periodic motion sliding at a slow speed to the periodic one synchronized to the vibration of the wobbling mass with increase of the wobbling frequency, ω. The average moving speed can be controlled indirectly based on entrainment to the wobbling motion at sufficiently-high wobbling frequencies. For achieving this, in this paper we introduced an intuitive wobbling motion following a sinusoidal trajectory, but more appropriate trajectory should be designed taking the motion optimality into account. Optimum design of the robot's body shape for exploiting the wobbling motion is also an issue to be investigated.

Through mathematical and numerical analyses in this paper, two interesting questions have been raised. One is the transition mechanism of the dominant dynamics according to the sliding frictional coefficient, the wobbling frequency, and the robot's body shape. The other is the problem of how the rotation and sliding motion balance at the contact position with a certain value of μ_0. Deeper understanding of these mechanisms is one of the major issues in the future.

REFERENCES

[1] F. Asano, Y. Kikuchi and M. Shibata, "Modeling, control and analysis of limit cycle walking on slippery road surface," *Int. J. of Dynamics and Control*, Vol. 2, Iss. 4, pp. 463–473, 2014.

[2] F. Asano, T. Saka and T. Fujimoto, "Passive dynamic walking of compass-like biped robot on slippery downhill," *Proc. of the Int. Conf. on Intelligent Robots and Systems*, pp. 4113–4118, 2015.

[3] F. Asano and I. Tokuda, "Indirectly controlled limit cycle walking of combined rimless wheel based on entrainment to active wobbling motion," *Multibody System Dynamics*, Vol. 34, Iss. 2, pp. 191–210, 2015.

[4] N. Maheshwari, X. Yu, M. Reis and F. Iida, "Resonance based multi-gaited robot locomotion," *Proc. of the IEEE/RSJ Int. Conf. on Intelligent Robots and Systems*, pp. 169–174, 2012.

[5] K. M. Lynch, N. Shiroma, H. Arai and K. Tanie, "The roles of shape and motion in dynamic manipulation: the butterfly example," *Proc. of the IEEE Int. Conf. on Robots and Automation*, Vol. 3, pp. 1958–1963, 1998.

[6] F. Asano, Z.-W. Luo, M. Yamakita and S. Hosoe, "Dynamic modeling and control for whole body manipulation," *Proc. of the IEEE/RSJ Int. Conf. on Intelligent Robots and Systems*, pp. 3162–3167, 2003.